Wear 330-331 (2015) 338–347

Contents lists available at ScienceDirect

Wear

journal homepage: www.elsevier.com/locate/wear

HVOF sprayed coatings of nano-agglomerated tungsten-carbide/cobalt powders for water droplet erosion application

M.S. Mahdipoor [a,*], F. Tarasi [a], C. Moreau [a], A. Dolatabadi [a], M. Medraj [a,b]

[a] Department of Mechanical Engineering, Concordia University, 1455 De Maisonneuve Blvd. West, H3G 1M8, Montreal, QC, Canada
[b] Department of Mechanical and Materials Engineering, Masdar Institute, Masdar City, P.O. Box 54224, Abu Dhabi, United Arab Emirates

ARTICLE INFO

Article history:
Received 15 September 2014
Received in revised form
9 February 2015
Accepted 11 February 2015

Keywords:
WC–Co
HVOF spray coating
Hardness
Toughness
Water droplet erosion

ABSTRACT

Water droplet erosion damage is due to the high speed impingement of several hundred micron-sized water droplets on solid surfaces. Thermal sprayed tungsten carbide based coatings show potential to combat such erosion problems. However, there are considerable discrepancies about their erosion performances in the literature. In the present work, the microstructure, phase composition and mechanical properties (micro-hardness and fracture toughness) of WC–Co coatings are studied in relation to their water droplet erosion performance. Coatings were deposited by high velocity oxygen fuel (HVOF) process and they were tested as-sprayed in WDE erosion system. The nano-agglomerated WC–Co powders are in either sintered or non-sintered conditions. The WDE tests were performed using 460 μm water droplets at 250, 300 and 350 m/s impact velocities. The coating with homogeneous microstructure shows up to 7 times less erosion rate than Ti6Al4V, while the coating with heterogeneous microstructure shows worse erosion rate compared to Ti6Al4V.

1. Introduction

Liquid erosion, often reported as a source of part failure in the power generation plants is a material damage caused by repeated impacts of a water droplets at high relative velocities [1,2]. In the case of water as the impinging fluid, the solid surface encounters hydrodynamic forces resulting from the impingement of water droplets of several hundred-micron sized at hundreds of meters per second relative velocities [1].

Different approaches have been studied to combat water droplet erosion (WDE) such as laser surface treatments or thermal spray coatings [3,4]. Cermet coatings consisting of a ductile metallic binder and a hard phase (e.g. carbide, boride, nitride) are among the promising solutions to this problem [4,5]. Tungsten carbide cobalt (WC–Co) cermet spray coatings are widely used for different applications which require abrasion, sliding, fretting and erosion resistance [4–7]. In this composite structure, the hard carbide particles cause high hardness, while the metallic binder provides the coating toughness. The mechanical properties of these coatings are greatly affected by the processing parameters and final microstructure [7].

WC–Co coatings are mainly fabricated by thermal spraying techniques where the feed powder particles are injected into a hot flame generated by a heat source. They are next propelled at high velocities toward the substrate to form splats that stack on each other and generate the coatings. Thermal spray processes involve high-turbulence flow of material (gases, molten, semi-molten and/or solid particles) and high cooling rates [8]. Therefore, they often suffer from some common flaws in the resulting microstructures such as porosity, crack, low inter-splat adhesion and unstable interface between the matrix and hard reinforcement [8,9]. Numerous studies have been done to improve coatings' properties by the choice of process, optimization of the process parameters and modifying the feedstock [7–10].

In addition to microstructural flaws, undesirable chemical and metallurgical reactions leading to the phase transformations are other major issues in thermal spray coating of these cermets. During spraying WC–Co powder, the agglomerated particles are heated at high temperature by the flame, the Co melts and dissolves a part of WC. The rapid cooling of the molten particles upon deposition causes the formation of regions of amorphous phases due to the short time for crystallization of the multicomponent phase (Co–C–W–O) [10–12]. The W_2C phase can precipitate around the original WC grains and, in case of severe oxidation and decarburization, W precipitates close to the interface of splats [11]. Impacts of these particles on the substrate make them to be flattened and cement them in the cobalt binder splats. WC surrounded by molten cobalt can be well bonded in the middle of the splats due to appropriate wetting by the binder. It is

* Correspondence to: Department of Mechanical and Industrial Engineering, Concordia University, 1455 de Maisonneuve Boulevard West, H3G 1M8, Montreal, QC, Canada.
E-mail address: m_mahdip@encs.concordia.ca (M.S. Mahdipoor).

http://dx.doi.org/10.1016/j.wear.2015.02.034
0043-1648/

noteworthy that oxidized carbide grains have lower wettability for Co binder and can result in weak bonding between the two components [11,12]. Moreover, oxidized particle prevents the strong inter-splat bonding [12]. These chemical and metallurgical reactions strongly depend on the velocity and temperature of the spray particles [8,13]. They can impair the mechanical properties specially the fracture toughness which is an important parameter for wear and erosion resistance [14].

High Velocity Oxygen Fuel (HVOF) spray process has been widely used to deposit WC–Co coatings. In this process, the fuel (in the form of gas or liquid) and oxygen are injected into a combustion chamber where they ignite and generate the heat for melting and the momentum to propel the particles toward the substrate. Moderate process temperature (up to 3000 K) and high particle velocity (up to 800 m/s) in HVOF result in desired properties for these coatings [8,9]. High density, strong adhesion between coatings and substrates, high inter-splat adhesion, limited chemical reactions during the coating process, and compressive residual stresses are the main advantages supplied by HVOF [9]. It is noteworthy that the compressive residual stresses would be beneficial for the applications which experience dynamic loading such as water droplet erosion [4].

Four primary damage modes have been proposed for WDE including plastic deformation and asperities formation, stress wave propagation, lateral outflow jetting and hydraulic penetration [1,2]. The impact pressures and subsequent imposed stresses result in shock waves which travel through the material. This sudden shock waves can cause initiation of micro-cracks, or further development of the pre-existing internal flaws such as cracks and porosities [1,2]. The cracks merge together and result in material removal. Plastic deformation and stress wave propagation mainly cause surface and subsurface cracking; and lateral outflow jetting and hydraulic penetration mainly cause development of the existing cracks [1,16]. Hardness, ductility, fracture toughness and fatigue limit have been mentioned as the main material properties influencing WDE performance. However, there is no complete agreement on their influence [1,16]. Among these properties, hardness of target material plays relatively more significant role by delaying the deformation. Ductility is another criterion leading to accommodation of localized stress concentration [6]. A suitable combination of hardness and ductility can manifest itself in the fracture toughness which is the most relevant mechanical property to erosion resistance of spray coatings [5,7].

Lima et al. [7] reported that the fracture toughness is the most relevant material property corresponding to the erosion resistance of WC–Co spray coatings; and the hardness would be a less important parameter. Lathabai et al. [17] mentioned that solid particle erosion of cermet coatings is not a function of their hardness. They found that coatings with low porosity, fine grain or splat size, absence of cracks and good inter-splat bonding show high erosion resistance. Oka et al. [5] investigated the water droplet erosion behavior of different ceramics, cermet spray coating and martensitic stainless steel. They reported much less erosion rate and much longer incubation period for WC–20Cr_3C_2–7Ni coating compared to stainless steel. Mann et al. [4] studied the water droplet erosion of HVOF sprayed WC–Co coatings in comparison with Ti6Al4V and stainless steel at low impact speeds. They observed excellent erosion resistance for the WC–Co when they used a modified coating process. It was mainly attributed to the compressive residual stress introduced into the coating as well as its high hardness and toughness. It is noteworthy that their erosion tests were carried out at 150 m/s impact speed which is not severe condition. Shipway et al. [2] also studied the water droplet erosion of WC–Co coatings sprayed by HVOF in comparison with Ti6Al4V. They used water jet cutting equipment to perform erosion experiments. The erosion test condition was very aggressive and the impact speed reached 830 m/s. In this case, the WC–Co coating did not show superior erosion resistance. They did not show any incubation period and they lost material faster than Ti6Al4V. The poor erosion resistance was attributed to the very aggressive erosion conditions and high impact speed. Water droplet erosion of WC–Co coatings was studied at either low impact speeds (150 m/s) or very high impact speeds (830 m/s). To the knowledge of the authors, there is no information related to their erosion performances for impact speeds within this range.

In the current study, water droplet erosion resistance of WC-12 wt% Co coatings is investigated. The utilized feedstock results in two different microstructures with same chemical composition for the final coatings. The impact speeds studied in the current work (250, 300, 350 m/s) are closer to the condition of water droplet erosion encountered in the compressor of gas turbine. The erosion behavior of coatings is discussed related to their microstructure and mechanical properties in order to understand the considerable difference for the erosion performance of WC–Co coating observed in the literature [2,4,5]. The erosion experiments are performed at three different droplet impingement speeds to explore the influence of this parameter on the erosion performance. The coatings' erosion behavior are compared with that of Ti6Al4V which is currently used as a compressor blade material and known to exhibit high resistance to water droplet erosion.

2. Experimental

2.1. Materials

Commercially available WC–Co powders Sulzer 5810 and Woka 3110, both from (Sulzer Metco Canada Inc. Fort Saskatchewan, AB) were used as the feedstock. Both feedstock are agglomerated powders and the major difference between the two is that only Woka 3110 powder is sintered following agglomeration. The chemical composition and particle size of the powders are summarized in Table 1. To avoid confusion, WC grains are referred to as “grains” and the agglomerates are referred to as “particles”, in the rest of the paper. Coatings were sprayed on Ti6Al4V substrates that were precleaned in acetone and then blasted with 60 mesh alumina grits.

2.2. HVOF coating process

The feedstock of Sulzer 5810 and Woka 3110 were deposited using DJ 2600 HVOF gun (Sulzer-Metco). The Sulzer 5810 powder was sprayed at five different conditions and the best one in term of coating hardness and density was selected and presented in this paper. The in-flight particle temperature and velocity were measured as 1860 °C temperature and 660 m/s at 200, 350 and 560 SLM oxygen, air and hydrogen flow rates, respectively. In the case of Woka 3110, it was sprayed using the flow rates of 230, 370 and 680 SLM for oxygen, air and hydrogen, respectively. Woka 3110 spraying conditions (in-flight powder temperature and velocity) were optimized in order to obtain dense and homogeneous

Table 1
Chemical composition of the feedstock used in the experiments.

Materials	Shape	Particle size (diameter) distribution (μm)	Chemical composition
Sulzer 5810	Spherical (agglomerated)	−63+11	WC, 12 wt% Co
Woka 3110	Spheroidal (agglomerated, sintered)	−25+5	WC, 11–13 wt% Co

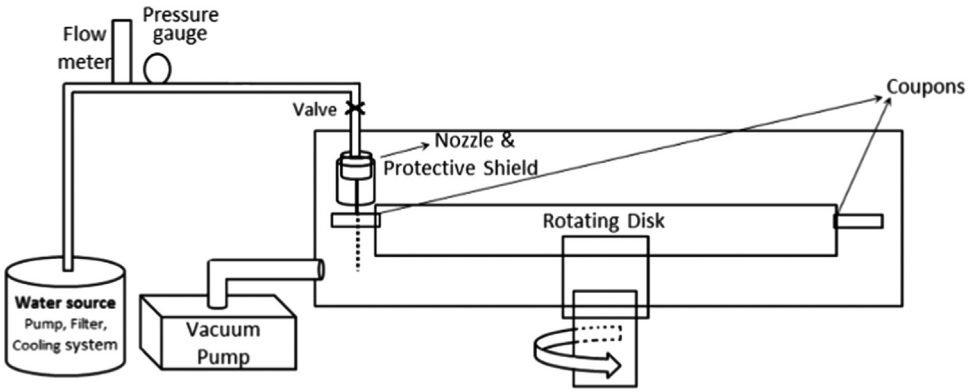

Fig. 1. Schematic of the water droplet erosion rig.

coatings [18]. The temperature and velocity of in-flight particles were 1986 °C and 730 m/s. Since, linking the erosion behavior of coating to its microstructure is among the objectives of this study, Woka 3110 and Sulzer 5810 coatings will be compared further. In this paper Woka 3110 coating is called SD and Sulzer 5810 coating is called SP.

2.3. Coating characterization

To evaluate the coating porosity, SEM images of coating cross section taken at low magnification, were analyzed using Scion Image software (Version 4.0.3.2). The mean surface roughness (R_a) values of as-sprayed coatings was measured using surface roughness tester (Mitutoyo SJ-210). The phase constituents of the coatings were analyzed using an X-ray diffraction (XRD). The micro-hardness was measured on coating cross sections using a Vickers micro-hardness tester with a diamond Vickers indenter under 500 g load. The reported micro-hardness values are the mean value of 5 measurements. Moreover, fracture toughness measurements were performed using Vickers hardness tester at 10 kg load. In order to find the fracture toughness from the indents dimension, following Eq. was utilized [15]:

$$K_{IC} = 0.0193 H_v D (E/H_v)^{2/5} a^{-1/2} \quad (1)$$

where H_v is the Vickers hardness, E the Young's modulus, D the half-diagonal of the Vickers indentation, and a the indentation crack length.

2.4. Water droplet erosion test

An erosion rig specially designed for WDE testing, which provides simulated impingement conditions of high speed rotating blades was used in this study. Fig. 1 illustrates a simplified schematic of the erosion rig. The erosion test coupons are mounted on the rotating disk and pass in front of the flow of water droplets emerging from a nozzle of specified size. The rotating coupons are impinged normally by the falling water droplets and experience water droplet erosion. The rotating disk can reach a maximum speed of 20,000 rpm, which corresponds to a linear impact speed of 500 m/s for the impingement of the water droplet on the specimen. The erosion tests are performed in vacuum pressure between 30 and 50 mbar for all experiments in order to balance friction and water droplet evaporation issues. To provide the desired impacting droplet sizes different nozzle sizes can be mounted on the system; and rotation speed is set based on the desired impact velocity.

To present the erosion results, the cumulative material loss curves were plotted vs. cumulative erosion exposure. Also, the maximum erosion rate (ER_{max}) of coatings and Ti6Al4V were determined according to the ASTM G73-10 standard [19]. A straight line is drawn using the maximum slope points from which the maximum erosion rate (ER_{max}) is calculated. In this paper, the vertical access of erosion graphs is the volume loss normalized by the area exposed to water droplets which corresponds to the mean depth of erosion. The horizontal access or erosion exposure was presented using the normalized volume of impacting water by the area exposed to water droplets. Such area was measured from the optical micrographs of eroded specimen recorded at the beginning of the maximum erosion rate stage. It is assumed to be the average of damaged surface area during the whole erosion experiment. Accordingly, the maximum erosion rate or mean depth of erosion rate is dimensionless.

The erosion tests were performed on the as-sprayed coatings without prior surface polishing or grinding. The incubation stage in erosion curve is a function of surface roughness and since the surface roughness is different for the coatings and Ti6Al4V bulk material, the incubation stage characteristics are not compared in this study. Here, the maximum erosion rate is reported as the main criterion for the erosion resistance.

2.5. Microstructural characterization

The cross section of cermet coatings were observed under a scanning electron microscope (SEM Hitachi S-3400N) to confirm their thickness and study their morphology and microstructure. Moreover, the cross section of eroded coatings were prepared for metallography at the same position along the erosion craters. From each cross section, more than 30 SEM images were taken at different magnifications along the edge of the erosion lines. Hence, erosion features could be studied systematically.

3. Results

3.1. As-sprayed coatings' characterization

Fig. 2 shows the XRD spectra of the cermet feedstock and coatings deposited by HVOF. The as-received Sulzer 5810 and Woka 3110 powders are composed of WC and Co phases. The XRD patterns of the coatings show the presence of other phases which are formed due to the spraying process. The SP coating contains W_2C and small amount of W, however the Co peaks are no more visible. Formation of W_2C and W confirms that the WC phase is decomposed and decarburized during HVOF process of Sulzer 5810 feedstock. The initial free Co could not be detected in the coating probably because it has reacted with carbon and tungsten during the coating process and formed nano-crystalline $Co_xW_yC_z$ phases as well as amorphous Co (W,C) [11,18]. The $Co_xW_yC_z$ were not detected by XRD because of their relatively small quantities. In the case of SD coating, it is also composed of WC, W_2C, W and some amorphous phases. However, there is a higher level of decomposition and

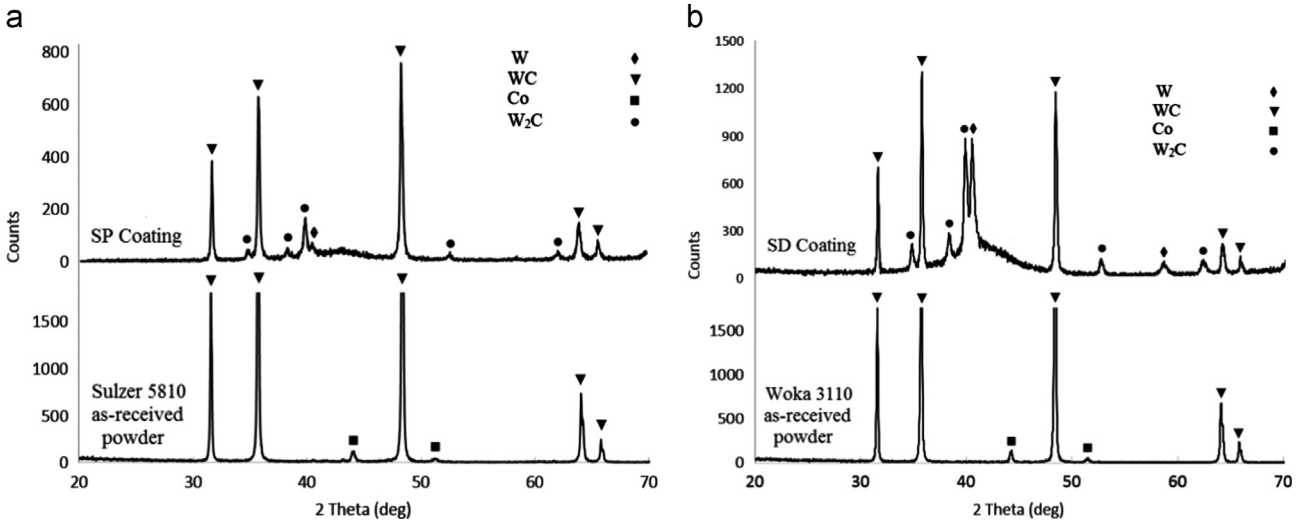

Fig. 2. XRD patterns of: (a) Sulzer 5810 powder and SP coating, (b) Woka 3110 powder and SD coating.

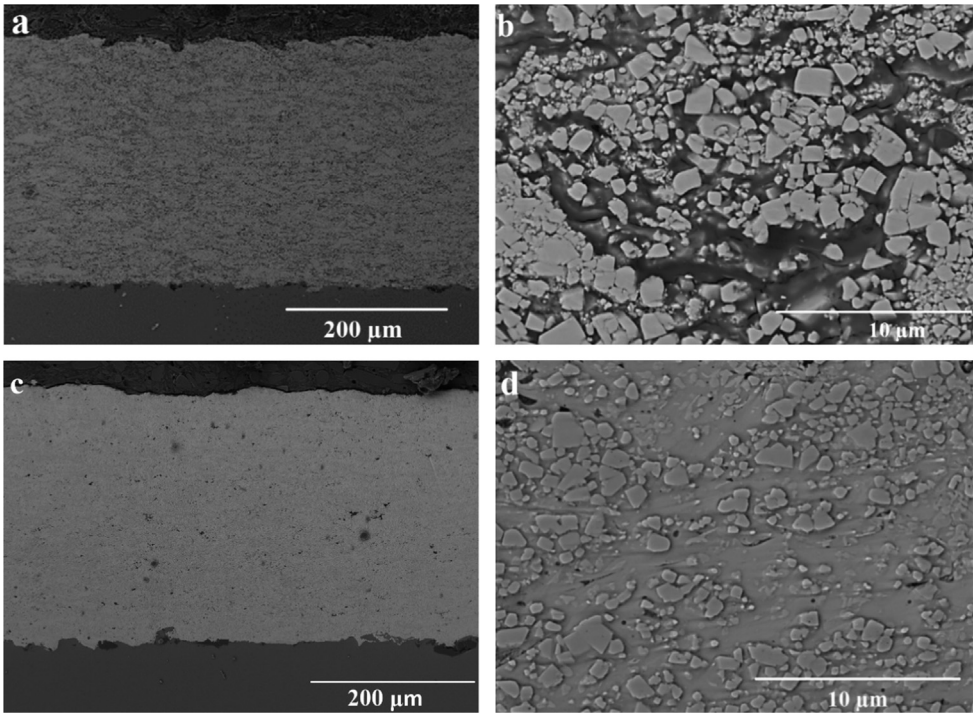

Fig. 3. SEM micrographs showing cross sections of as-sprayed: (a) SP coating at low magnification, (b) SP coating at high magnification, (c) SD coating at low magnification, (d) SD coating at high magnification.

decarburization. This is shown by the higher peak intensity ratio of W_2C/WC in the pattern as well as larger amorphous hump observed between 35° and 45° representing greater amorphous content. Formation of W phase in the coating also confirms the higher degree of decarburization. These indicate higher melting proportion of the agglomerated and sintered Woka 3110 particles than that of Sulzer 5810 (which is only agglomerated) during deposition. It is in accordance with the higher measured temperature for in-flight Woka powders during the spraying process. High temperature would enhance the coating density; however, it would be detrimental for final mechanical properties, especially for its toughness. Marple and Lima [18] introduced an optimized in-flight powder temperature range, 1750–1950 °C, for different WC–Co feedstocks sprayed by HVOF. The temperatures of in-flight powder sprayed in the current work are in this optimized range.

Fig. 3 shows SEM micrographs of polished cross sections of spray coatings. The porosity percentage, thickness and surface roughness of the coatings are presented in Table 2.

The porosity and some macro-flaws mentioned as important parameters for mechanical properties can be seen in Fig. 3. It is evident that there is much less porosity in SD coating, which can be assumed as the first structural indicator for good erosion behavior. The surface roughness of the target material is another important parameter in erosion studies as it influences the initial stages of erosion significantly. The different roughnesses of the coatings and the bulk Ti6Al4V sample are mentioned in Table 2.

Mechanical properties of the coatings as well as Ti6Al4V are listed in Table 2. The SP coating shows much lower hardness compared to the SD coating. It is attributed to the larger variations in its microstructure and lower inter-splat adhesion which will be

Table 2
The characteristics of as-sprayed coatings.

Specimens	Macro-porosity percentage (%)	Thickness (μm)	Surface roughness, R_a (μm)	Micro-hardness ($HV_{0.5}$)	Fracture toughness (MPa $m^{1/2}$)
SP coating	2.9	360	3.62	874 ± 30	–
SD coating	1.4	330	2.03	1232 ± 14	8.2
Ti6Al4V	–	–	0.08	298 ± 26	60–100

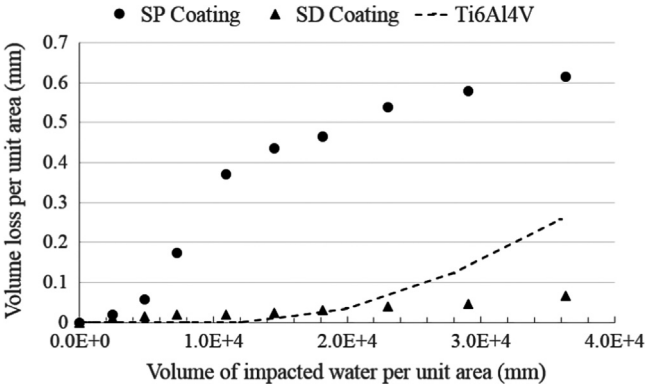

Fig. 4. Cumulative volume loss per unit area vs. cumulative volume of water impacting unit area at the impingement speed of 250 m/s.

discussed further. Fracture toughness could not be measured for SP coating since the cracks run along the edge of indents instead of radial cracking. This indicates the low tensile strength of this coating [12] which is in accordance with its heterogeneous microstructure (Fig. 2b) and low micro-hardness. This was not the case for SD coating and its fracture toughness was measured. The relatively high observed fracture toughness (8.2 MPa $m^{1/2}$) is in accordance with the dense and homogeneous microstructure of SD coating. However, high decarburization degree and formation of brittle and amorphous phases in this coating would cause reduction of fracture toughness.

3.2. Erosion results

The erosion behavior of the coatings and Ti6Al4V using 250, 300 and 350 m/s droplet impact speeds are presented in Figs. 4–6, respectively. Based on the ASTM standard, the maximum erosion rates were calculated from the erosion curves and they are listed in Table 3 at different erosion conditions.

Fig. 4 shows the erosion test results at 250 m/s impingement speed. It exhibits significant differences between the erosion behavior of the coatings and Ti6Al4V. The SP coating presents the highest erosion rate which is 3.7 times higher than that of Ti6Al4V. The SD coating demonstrated the best erosion performance in this condition since its erosion rate is 6.7 times lower than that of Ti6Al4V.

The erosion results for the impact speed of 300 m/s are shown in Fig. 5. There is a remarkable difference between the erosion behavior of the coatings at this speed and that at 250 m/s impact speed. No incubation period was observed for the coatings at 300 m/s. This can be attributed to the higher impact pressure and subsequent stresses generated at 300 m/s that are sufficiently high to initiate damage in the coating at the beginning of erosion test. In term of erosion rate, the ER_{max} of SP coating is close to Ti6Al4V. i.e. 7×10^{-5} and 5.2×10^{-5}, respectively. However, SD coating shows significantly lower erosion rate, which is 1.9×10^{-4} (Table 3). It is 2.6 and 3.5 times less than the erosion rates of Ti6Al4V and SP coating, respectively.

Fig. 6 shows the results for the most aggressive erosion conditions that is 350 m/s impact speed. The erosion curves are closer to each

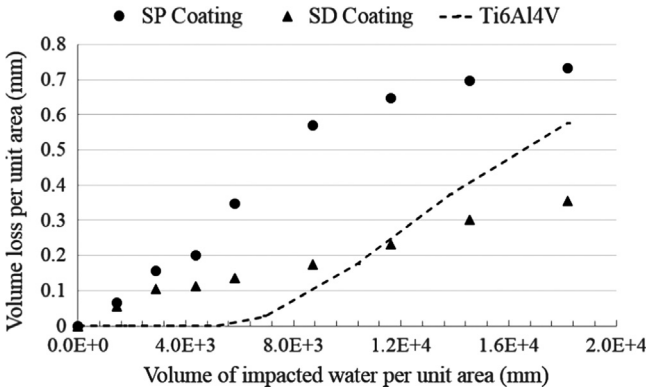

Fig. 5. Cumulative volume loss per unit area vs. cumulative volume of water impacting unit area at the impingement speed of 300 m/s.

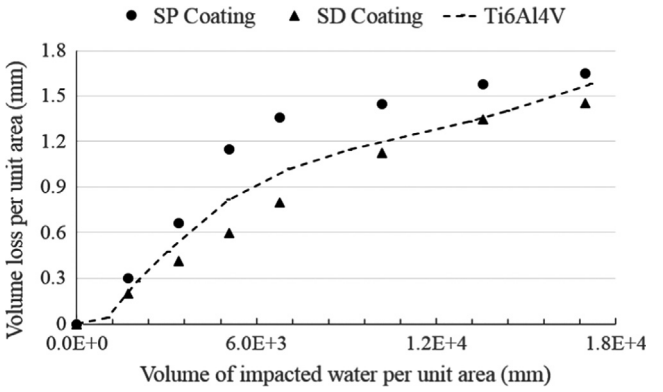

Fig. 6. Cumulative volume loss per unit area vs. cumulative volume of water impacting unit area at the impingement speed of 350 m/s.

other at this speed. The maximum erosion rates ER_{max} are 1.9×10^{-4}, 2.51×10^{-4}, and 1.17×10^{-4} for Ti6Al4V, SP and SD coatings, respectively. The erosion rate for the SP coating is higher than that of Ti6Al4V; however, SD coating again exhibits a lower erosion rate.

It is evident that SD coating shows the least ER_{max} in all erosion conditions. Although the coatings were deposited from feedstock with identical chemical compositions, the erosion resistance of SP coating is much less than that of SD coating. Explaining this significant difference in coating erosion behavior which is also reported in the literature [2,4] is one of the objectives in this study. To this end, microstructural characteristics and erosion mechanism investigation were performed.

3.3. Microstructural characteristics of eroded coatings

To reveal the influence of the coating's morphology and microstructure on the processes leading to material removal scanning electron microscope was utilized. Fig. 7 shows the cross sectional view of the complete erosion crater. The width of the erosion line was roughly measured and the approximate width average was found to be 1.18 mm for SP coating and 0.94 mm for SD coating; however, it was 0.82 mm for Ti6Al4V in the same stage. These widths are more than two times the droplet diameter of 460 μm. The smooth surface of the coating erosion craters is a notable feature which cannot be seen with the Ti6Al4V alloy. The topography of the eroded surface can play a vital role in the progress of the erosion damage and the processes causing erosion saturation [3]. During the erosion test, a thin film of water would cover the eroded areas and acts as a cushion leading to a decrease of the imposed impact pressure [1,3]. The erosion texture influences the water film formation and its cushion role. Therefore, it should be considered in order to investigate the water droplet erosion mechanism.

Table 3
Maximum erosion rate (ER_{max}) of the coatings and Ti6Al4V.

	ER_{max}, 250 m/s (mm^3/mm^3)	ER_{max}, 300 m/s (mm^3/mm^3)	ER_{max}, 350 m/s (mm^3/mm^3)
SP coating	5.2×10^{-5}	7×10^{-5}	2.51×10^{-4}
SD coating	2.1×10^{-6}	1.9×10^{-5}	1.17×10^{-4}
Ti6Al4V	1.4×10^{-5}	5.2×10^{-5}	1.9×10^{-4}

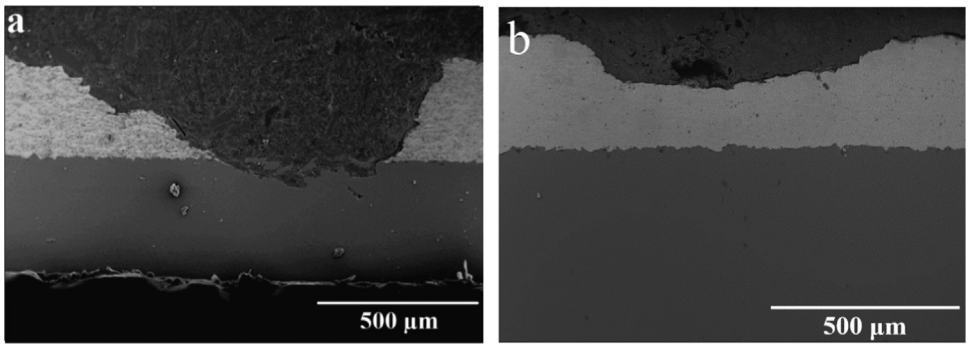

Fig. 7. Cross-sectional SEM images showing the depth and texture of the erosion craters at impact speed of 250 m/s: (a) SP coating, (b) SD coating.

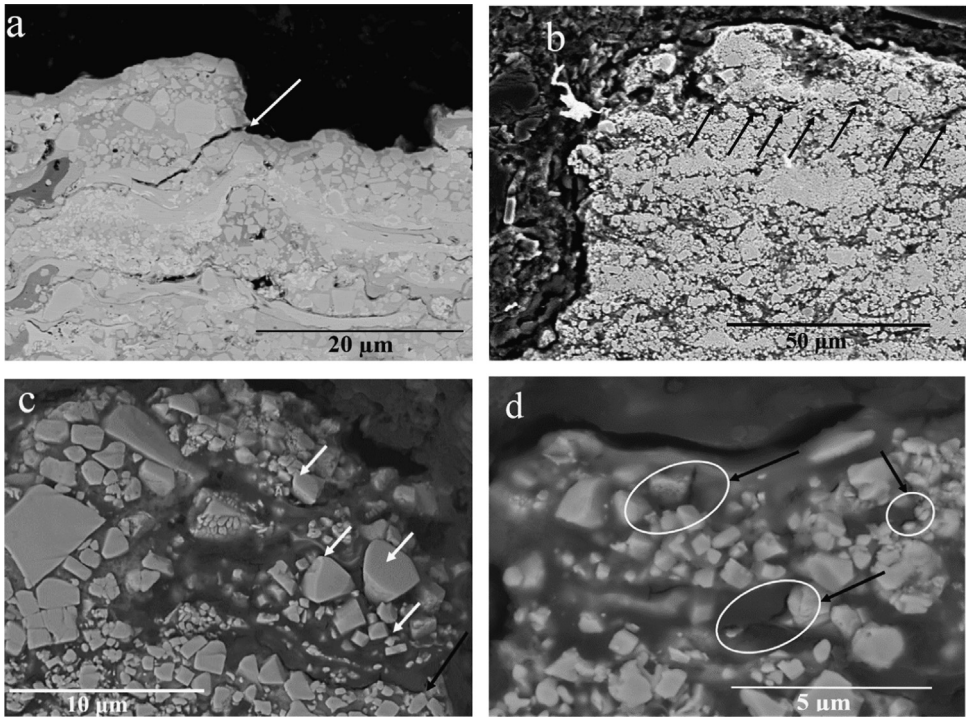

Fig. 8. Cross sectional SEM images of eroded SP coating along the edges of erosion crater, WDE conditions: 460 µm droplet size and 300 m/s impact speed.

Fig. 8 shows the SEM images of erosion crater along its edges for SP coating. The splat microstructure and high density internal flaws close to the erosion line can be identified in Fig. 8a and b. The surface and sub-surface cracks, which are known mechanisms for WDE damage [2,20], were observed (indicated by arrows). This cross sectional view presents only a two-dimensional view of a three dimensional erosion track. There are several cracks, as shown in Fig. 8d, which are very small relative to the other surrounding microstructural features. They are considered as nucleated cracks formed mainly at interface between the hard reinforcement WC grains and the Co binder (black arrows, Fig. 8d) or at the interface between different splats (black arrows, Fig. 8c). Fig. 8b shows a network of sub-surface cracks right on the edge of the erosion crater. These cracks may nucleate due to the fracture of WC particles and their coalescence leads to detachment of large fragments of the coating. The cracks mainly initiated between the splats and some un-molten particles. As mentioned, SP coating does not show a homogenous microstructure; and low adhesion at the splat interfaces has left numerous internal flaws. These flaws, such as pre-existing cracks, grow significantly when receiving stress waves upon water droplet impingement. In addition, the detachment of WC grains from the cobalt binder and also their cracking are observed along the erosion line edge as shown in Fig. 8d.

Fig. 9 shows cross sectional images of SD coating following WDE. The coating splat structure beside the damaged areas can hardly be

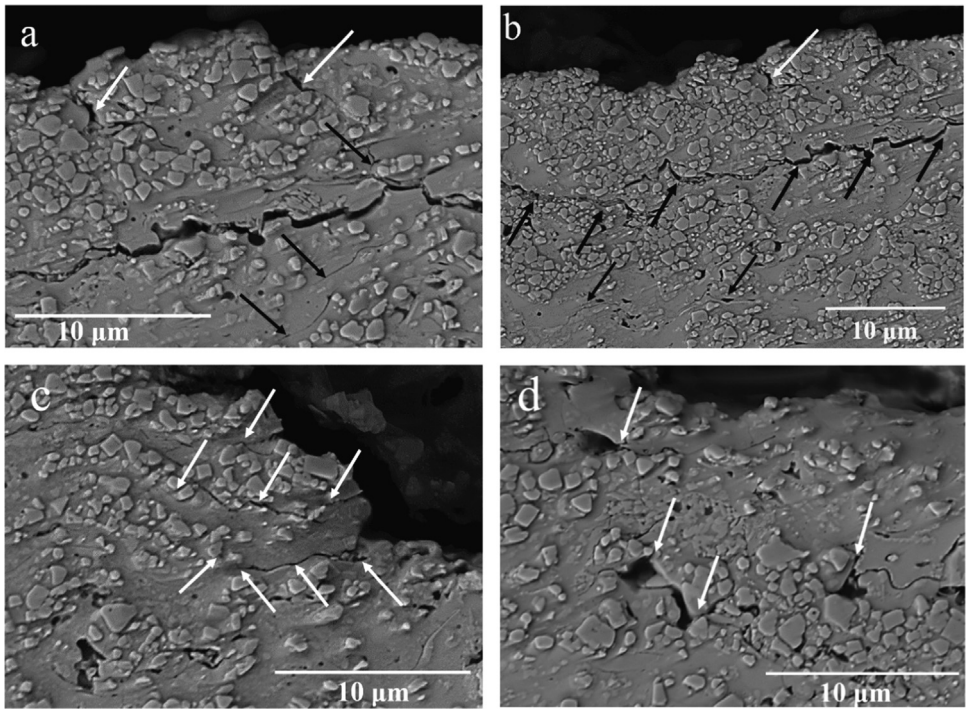

Fig. 9. Cross sectional SEM images of eroded SD coating along the edges of erosion crater, erosion conditions: 460 μm droplet size, 300 m/s impact speed.

identified because the microstructure is much more homogenous. Because of intense pressure of each water droplet impingement and subsequent stress wave propagation, the surface (white arrows) and sub-surface (black arrows) micro-cracks are formed as illustrated in Fig. 9a and b. They propagate and merge together and form large sub-surface cracks which result in detachment of large lumps of the coating as shown in Fig. 9b. The sub-surface lateral cracking was observed during the solid particle erosion of brittle materials and highlighted as one of the dominant fracture mechanisms leading to material loss [20]. Moreover, a network of macro and micro-cracks can be seen in Fig. 9c. There is a very high chance for detachment of materials from this kind of crack networks by the repeated impingements. Fig. 9d shows cracking from pre-existing pores due to the high stress concentration around these defects in the coating microstructure. One can discern the WC–Co structure in the middle of the splats and note the excellent cohesion between the WC grains and binder. Here, the amorphous binder at the periphery of the splats is detrimental for their adhesion. The micrograph shows presence of cracks mainly between splats.

Clearly, the density of internal flaws in SP coating is larger than that of SD coating. Also, the amount of nano-pores and micro-pores in the former coating is much higher. Low coating hardness is usually attributed to high porosity. However, the porosity reported in Table 2, corresponds only to micro-porosity and is too low to account for the low hardness of SP coating. In this coating, the low cohesion of WC/Co bonds causes the formation of high density zones of nano-pores around the WC grains. They were not considered in the porosity values listed in Table 2, but they contribute to the low observed hardness and result in worse erosion performance.

4. Discussion

4.1. Water droplet erosion damage

The water droplet impacts with high relative velocity cause damage to all materials. Different mechanisms for WDE have been found and described. They depend on the target material properties and water droplet impact conditions [1,2,16]. The magnitude of impact pressure and subsequent stress waves propagating through the material is a function of impact speed which is summarized in the following well-known equation [16]:

$$P_{impact} = \rho_0 C_0 V_0 \tag{2}$$

where ρ_0 is the liquid density, C_0 is the speed of sound in the liquid and V_0 is the impact speed. The accuracy of Eq. (2) is limited due to the applied simplifications. Heymann [22] did some modifications and proposed the following equation which is used in the current study:

$$P_{impact} = \rho_0 C_0 V_0 \left[2 + (2k-1)\frac{V_0}{C_0}\right] \tag{3}$$

where k is liquid constant. In the case of water erosion, $k=2$, $\rho_0 = 1000\ \mathrm{kg/m^3}$ and $C_0 = 1463$ m/s. Therefore, the impact speeds of 250, 300, and 350 m/s correspond to impact pressures of 919, 1147, and 1391 MPa, respectively.

The remarkable influence of impact pressure on the erosion behavior of coatings manifests in the erosion curves (Figs. 4–6). Fig. 4 illustrates the erosion behavior of the coatings and Ti6Al4V bulk material at 250 m/s. It can be seen that impact pressure of 919 MPa could not impose enough stresses on SD coating to cause notable material removal. Cracking in this condition was very slow and required a large number of impingements. In contrast, shorter incubation period in erosion of SP coating confirms that the shock pressure caused faster cracking and material loss in the microstructure of this coating.

At higher droplet impact speed, i.e. 300 m/s that translates to impact pressure of 1147 MPa, the stress was enough to cause material removal from early stages for both coatings. However, they did not show the same material removal rate. SD coating exhibits lower erosion rate due to its denser and more homogenous microstructure as shown in Fig. 9. In this coating, crack development among the well bonded splat boundaries required higher stress and was slow. However, the cracking at the weak interfaces of SP coating microstructure was faster and require lower energy.

When erosion experiments were performed at 350 m/s impact speed, the impact pressure and subsequent stresses induced brittle

and catastrophic damage on both coatings. It seems that 1391 MPa impact pressure was quite high enough for cracking in either the interface of WC/Co or splat boundaries leading to large fragments material loss. Also, it could enlarge the pre-existing cracks easily in both coatings. In the case of spray coatings, the adhesion strength among the interfaces would determine the required stresses for crack propagation. Indeed, the interaction between these required stresses and the stress waves resulted from droplet impacts causes the observed material loss. Hence, the different erosion testing conditions have a large influence on the variability of the reported erosion behaviors of WC–Co coatings in the literature [2,4,5].

It is known that the erosion resistance when plotted as material removal rate vs. the impact speed, resembles an *S–N* curve for fatigue from which the fatigue limit is defined. Such a concept in erosion behavior of some materials could be called as erosion limit [23]. It means that there is a threshold velocity below which the applied shock pressure cannot cause material loss within a certain time limit. In the current work, it seems that 919 MPa is close to the erosion limit of SD coating because of its relatively low material loss after more than 3 million droplet impacts. However, testing at lower impact speeds needs to be carried out to find the potential erosion limit of SP coating. Since both coatings have same chemical composition and grain size, it can be inferred that the coating microstructure determines its tolerable stress and erosion limit. Indeed, the microstructure is a function of utilized feedstock as well as coating process parameters and they should be optimized to achieve WDE resistant coating.

4.2. Erosion mechanism of spray coatings

In general, the WDE resistance of a target material has been related to its mechanical properties including resilience, hardness, toughness, elastic modulus, or ultimate tensile strength [1]. Erosion behavior of bulk alloys can be classified into two main groups: materials which fail in a brittle manner and those which deform plastically [16]. The erosion resistance of bulk materials such as titanium alloys was mainly related to their respective hardness [21]. Unlike titanium alloys, the erosion resistance of spray coatings was roughly related to their fracture toughness [5,7]. However, both hardness and fracture toughness apart from the chemistry of the material, significantly depend on the coating morphology and microstructure. Hence, the coating microstructure has to be assessed in detail to identify the erosion mechanism, especially because the coating mechanical properties are normally reported from specific locations in the material; while the erosion phenomenon involves the entire coating and can find the regions of weakness in the microstructure to initiate material removal.

Fig. 3a and b shows the microstructures of the as-sprayed SP coating having a heterogeneous microstructure with high density of pores. The carbide grains distribution is not uniform and their large accumulation can be seen in the coating. The XRD results show the low degree of decarburization for SP coating. This is confirmed also by the angular shape of WC grains which indicates regions stayed solid throughout the coating process. The partial melting of particles can be attributed to the low density of 5810 powders and their low thermal conductivity. Indeed, the temperature of in-flight particles at the center is lower than at the surface and as a result some parts may not be molten. This has led to the heterogeneous microstructure of SP coating. Low level of carbon and tungsten dissolution in the cobalt decreases the amount of inter-diffusion of cobalt into WC grains and vice versa resulting in reduced wetting between the WC grains and the binder. The low adhesion of WC grains and cobalt binder forms a large number of micro and nano-pores (Fig. 8d). The high level of internal defects are consistent with the measured micro-hardness for SP coating. As mentioned, fracture toughness of this coating could not be measured since the cracking happened along the edges and not at the corners of the indent. This type of cracking contributed to the low tensile strength and accelerated crack growth [12]. The higher crack growth rate explains the poor erosion behavior. Upon water droplet impacts, the stress waves propagate through the coating and they interact with microstructural flaws such as pre-existing cracks. These interactions lead to crack growth acceleration and increase the material loss rate. The incubation period and the accelerated erosion rate depend strongly on the presence of internal defects. According to SP coating microstructure, the micro-pores, micro-cracks, low adhesion of WC grains and cobalt, and the weak splat boundaries are flaws present in this coating. Once the stress waves propagate through the coating, the present cracks in the splat boundaries grow and cause material detachment (Fig. 8a). The poor bonding of WC and Co and resulting built-in pores cause the formation of many micro-cracks. The micro-cracks next form a crack network that results in material removal (Fig. 8b). Moreover, the micro cracking around the large WC grains would cause their direct detachment from the cobalt binder (Fig. 8c). In addition to individual detachment of carbide grains, because of the large accumulation of WC particles seen in this microstructure and their poor bonding with the Co binder, cracking occurs around these agglomerations and cause their group removal. The fracture of large WC particles as observed in the results expedites the material loss.

In the case of SD coating, there is a compact microstructure of well bonded WC grains into the binder which contributes to the higher hardness. The WC grains distribution is uniform and there is much less porosity leading to high fracture toughness. The optimized temperature and high velocity of in-flight powders result in relatively low porosity of this coating. Unlike SP coating, the adhesion of WC and Co is not the challenge for the erosion of this coating; but the inter-splat boundaries are the main issue. The higher in-flight powder temperature and uniform heat transformation among these sintered particles result in higher decarburization level which is confirmed by XRD results. Higher temperature also leads to enhanced wetting and adhesion between WC and Co. However, the higher the degree of decarburization, the lower the adhesion between the splats. This is due to the extra formation of undesired amorphous and brittle phases at the interfaces. They are clearly detrimental for fracture toughness and consequently for erosion resistance [12,13]. Accordingly, the main weaknesses point in this microstructure are the splat boundaries. During the WDE test, the pre-existing cracks in the splat interfaces propagate and open their way toward the other weak point of the structure i.e. inter-splat interfaces. There they develop much more rapidly and cause detachment of large fragments or the whole of the splats as shown in Fig. 9a and b. This phenomenon causes the detachment of complete or part of splats in the form of splat lifting. Although, recognizing different splats is difficult in the microstructure, the waviness of the observed cracks is a good way to verify the crack growth along the splat interfaces.

As in other thermal spray coatings, the role of the pores in this SD coating should not be ignored. Micro-pores are another internal flaw which cause cracking under hydrodynamic loading of erosion. Fig. 9d illustrates the crack initiation from the pores which are already present in the microstructure. It was found that these cracks behave like a network and merge together with consecutive impingements.

In advanced stage of erosion, the lateral outflow jetting and hydraulic penetration participate in the erosion damage more than in the initial stages. When a part of the coating is removed, the texture of the eroded surface becomes very important for the progress of erosion. In the case of rough surface, the droplet impacts can be more detrimental. For the splat microstructure of spray coatings, the interfaces exposed to water impact are the main damage initiation points. Fig. 10 illustrates a simple schematic representation of water droplet impingement on a spray coating with its splat microstructure. Upon water droplet impact with the surface, lateral water jet

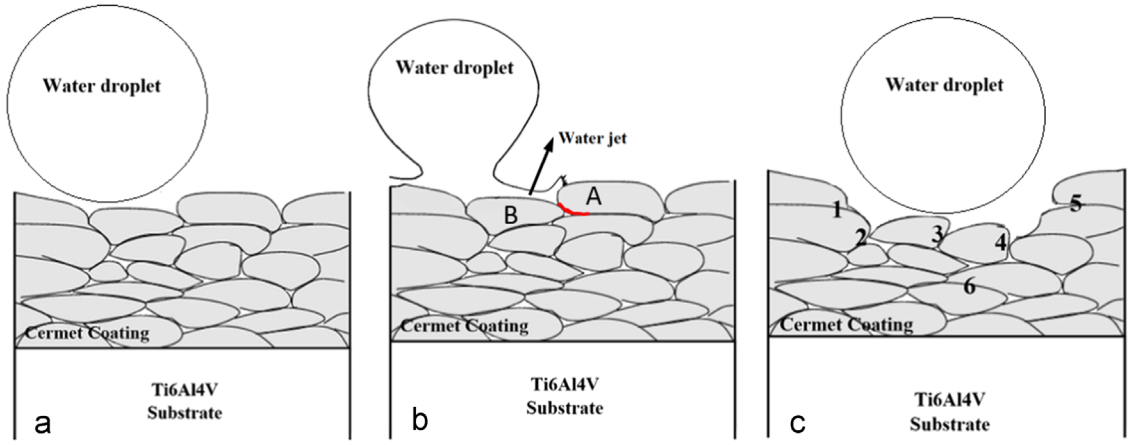

Fig. 10. Schematic of water impact on a cermet coating with its typical splat microstructure: (a) as-sprayed cermet coating before water impact, (b) upon impact and formation of water jet, (c) eroded cermet coating exposed to water droplet impingement in advanced stage.

forms and travels on the surface with very high speed. The water jet strikes any kind of irregularities on the surface such as raised splats and causes cracking. In Fig. 10b, water jet strikes the splat A and a micro-crack initiates at the interface of splat A and B. In advanced stages, when part of the coating was removed, a larger number of splat interfaces encounter the impacting water droplets. In this step, stress wave propagation, outflow jetting and hydraulic penetration contribute in erosion damage in parallel. However, there would be a high chance for sub-surface cracking by stress waves at positions such as number 6 which are beneath the center of impact and experience the maximum impact pressure. Number 1 and 5 zones which are close to the circumference of the impact area would be damaged by the formed lateral outflow jets. The splat interfaces would be opened up and it cause lifting of splats. In number 2, 3, and 4 areas, the hydraulic penetration would be dominant process for cracking and subsequent digging.

It was determined that the erosion damage of carbide cermet coatings is dominated by cracking. The erosion rate is controlled by cracks initiation and growth rate. Crack initiation was found to depend strongly on internal flaws. Crack growth rate was function of the adhesion strength in the coating. The droplet impact may cause carbide particle breaking, detachment of WC grains from the binder and lifting of splats. Indeed, the inter-splat adhesion strength plays a significant role on the crack growth rate and as a result the erosion rate.

It is noteworthy that the WDE behavior considerably depends on the surface roughness. Also, top layers of spray coating close to the surface show higher level of porosity compared to the underneath layers. Therefore, WDE performance of ground and polished SD coating will be compared with as-sprayed in a future publication.

5. Conclusions

In this study, the water droplet erosion behavior of WC–12Co sprayed coatings having two different microstructures was evaluated. To gain insight into the importance of erosion test parameters, WDE experiments were performed at three impact speeds. The erosion mechanism of the coatings was also investigated. The following conclusions can be drawn:

- Spraying commercial Woka 3110 powder and Sulzer 5810 powder resulted in two different microstructures for WC–12Co coatings. SD coating showed superior erosion performance compared to Ti6Al4V; however, SP showed less erosion resistance. Despite their identical chemical composition, the results show that the coating microstructure has a strong influence of WDE resistance and must be controlled carefully during spraying. In an optimum coating, the density of pores should be reduced, inter-splat adhesion and coating toughness should be maximized by limiting carbide degradation during spraying. They can be achieved by selecting appropriate feedstock and proper control of their temperature and velocity during spraying process.
- The spray cermet coating was eroded by different mechanisms depending on their microstructure and internal flaws. The main damage evolution process was cracking (surface and sub-surface) which was related to the coating fracture toughness. It involved carbide particles breaking, detachment of WC grains from the binder and lifting of the splats.
- The erosion damage of SD coating was governed mainly by splats lifting. The cracks propagation in the inter-splat boundaries followed by detachment of splats is the main process resulting in material loss. It is due to the stress wave propagation through the material. However, lateral outflow jetting and hydraulic penetration would accelerate this process in the later erosion stages.
- In the case of SP coating and its heterogeneous microstructure, erosion damage was operated by carbide particles breaking, detachment of WC grains from the binder and lifting of the splats in parallel and it was not possible to identify a dominant erosion mechanism.
- The water droplet impingement speed was found to have strong influence on the WDE performance of WC–Co spray coatings. The erosion rate of SP coating increased more than 100 time by increasing impact speed from 250 m/s to 350 m/s. In the case of SD coating, the potential erosion endurance limit in terms of impact speed should be located between 200 and 250 m/s.

Acknowledgments

The authors would like to acknowledge the help of Hany Kirols, Dmytro Kevorkov, Ahmad Mostafa of the Thermodynamics of Materials Group (TMG), Concordia University, for their valuable suggestions. They also wish to express their gratitude to Dr. R. Lima, National Research Council of Canada for supplying the HVOF spray coatings.

References

[1] F.J. Heyman, Liquid impingement erosion, in: S.D. Henry (Ed.), Wear ASM Handbook, vol. 18, 1992, pp. 221–232.
[2] P.H. Shipway, K. Gupta, The potential of WC-Co hardmetals and HVOF sprayed coatings to combat water-droplet erosion, Wear 271 (2011) 1418–1425.
[3] M. Ahmad, M. Casey, N. Sürken, Experimental assessment of droplet impact erosion resistance of steam turbine blade material, Wear 267 (2009) 1605–1618.

[4] B.S. Mann, V. Arya, P. Joshi, Advanced high-velocity oxygen-fuel coating and candidate materials for protecting LP steam turbine blades against droplet erosion, J. Materi. Eng. Perform. 14 (2005) 487–494.
[5] Y.I. Oka, H. Miyata, Erosion behaviour of ceramic bulk and coating materials caused by water droplet impingement, Wear 267 (2009) 1804–1810.
[6] B.S. Mann, V. Arya, HVOF coating and surface treatment for enhancing droplet erosion resistance of steam turbine blades, Wear 254 (2003) 652–667.
[7] M.M. Lima, C. Godoy, P.J. Modenesi, J.C. Avelar-Batista, A. Davison, A. Matthews, Coating fracture toughness determined by Vickers indentation: an important parameter in cavitation erosion resistance of WC–Co thermally sprayed coatings, Surf. Coat. Technol. 177–178 (2004) 489–496.
[8] S. Dallaire, M. Dufour, B. Gauthier, Characterization of wear damage in coatings by optical profilometry, J. Therm. Spray Technol. 2 (1993) 363–368.
[9] C. Verdon, A. Karimi, J.-L. Martin, A study of high velocity oxy-fuel thermally sprayed tungsten carbide based coatings. Part 1: microstructures, Mater. Sci. Eng. A 246 (1998) 11–24.
[10] D.A. Stewart, P.H. Shipway, D.G. McCartney, Microstructural evolution in thermally sprayed WC–Co coatings: comparison between nanocomposite and conventional starting powders, Acta Mater. 48 (2000) 1593–1604.
[11] J.M. Guilemany, J.M. de Paco, J. Nutting, J.R. Miguel, Characterization of the W_2C phase formed during the high velocity oxygen fuel spraying of a WC+12 Co powder, Metall. Mater. Trans. A 30 (1999) 1913–1921.
[12] Y. Qiao, T.E. Fischer, A. Dent, The effects of fuel chemistry and feedstock powder structure on the mechanical and tribological properties of HVOF thermal-sprayed WC–Co coatings with very fine structures, Surf. Coat. Technol. 172 (2003) 24–41.
[13] B.R. Marple, J. Voyer, J.F. Bisson, C. Moreau, Thermal spraying of nanostructured cermet coatings, J. Mater. Process. Technol. 117 (2001) 418–423.
[14] M. Jafari, M.H. Enayati, M. Salehi, S.M. Nahvi, C.G. Park, Microstructural and mechanical characterizations of a novel HVOF-sprayed WC-Co coating deposited from electroless Ni–P coated WC–12Co powders, Mater. Sci. Eng. A 578 (2013) 46–53.
[15] K. Nihara, A fracture mechanics analysis of indentation-induced Palmqvist crack in ceramics, J. Mater. Sci. Lett. 2 (1983) 221–223.
[16] G.S. Springer, Liquid Droplet Erosion, John Wiley & Sons, New York, 1976.
[17] S. Lathabai, M. Ottmuller, I. Fernandez, Solid particle erosion behaviour of thermal sprayed ceramic, metallic and polymer coatings, Wear 221 (1998) 93–108.
[18] B.R. Marple, R.S. Lima, Process temperature/velocity hardness wear relationships for high velocity oxyfuel sprayed nanostructured and conoventional cermet coatings, J. Therm. Spray Technol. 14 (2005) 67–76.
[19] ASTM Standard G73, 2010, Standard test method for liquid impingement erosion using rotating apparatus, ASTM International, West Conshohocken, PA, 2010, http://dx.doi.org/10.1520/C0073-10, ⟨www.astm.org⟩.
[20] A.G. Evans, T.R. Wilshaw, Quasi-static solid particle damage in brittle solids—I. Observations analysis and implications, Acta Metall. 24 (1976) 939–956.
[21] K. Tsubouchi, N. Yasugahira, S. Yoshida, R. Kaneko, T. Sato, Evaluation of water droplet erosion for advanced large steam turbine, ASME, New York, NY, United States 10 (1990) 245–251.
[22] F.J. Heymann, On the shock wave velocity and impact pressure in high-speed liquid-solid impact, Trans. ASME 90 (1969) 400–402.
[23] A. Thiruvengadam, S.L. Rudy, M. Gunasekaran, Experimental and analytical investigations on multiple liquid impact erosion, NASA CR-1638, 1970.